Journal of Sound and Vibration (2003) **259**(2), 299–322
doi:10.1006/jsvi.2002.5162, available online at http://www.idealibrary.com on IDEAL®

SOUND TRANSMISSION THROUGH ELASTOMERIC BULB SEALS

J. Park, T. Siegmund and L. Mongeau

1077 *Ray W. Herrick Laboratories, School of Mechanical Engineering, Purdue University, West Lafayette, IN* 47907-1077, *USA. E-mail: mongeau@ecn.purdue.edu*

(*Received* 21 *June* 2001, *and in final form* 18 *February* 2002)

The sound barrier performance of elastomeric vehicle weather seals was investigated. Experiments were performed on a single bulb seal specimen using a reverberation room method. The seal wall velocity was measured using a laser Doppler vibrometer. The sound pressure near the velocity measurement location was measured simultaneously, which allowed the sound intensity on both sides of the seal and the sound transmission loss to be determined. The vibration response and the sound transmission loss of the bulb seal were then computed using finite element analysis. Acoustic–structure interactions were considered for a partially coherent spatially distributed pressure excitation. The experimental data obtained using the reverberation room method allowed the validation of the numerical models. The resonance frequency due to the mass–air–mass mode of vibration was accurately predicted. The model was then used to numerically investigate the influence of various design parameters. It was found that the elastic modulus significantly affects the bulb seal resonance frequency, and that the loss factor of the material has major effects on the sound transmission loss around resonance.

1. INTRODUCTION

Weather seals are used in automobiles to prevent water and air from flowing through gaps around doors, windows, and other closure systems. The main sealing systems include: glass run seals around passenger side-glass windows, inner and outer belt line seals along the interface between side-glass windows and the doors, lift gate seals and primary bulb seals located around the periphery of the hatch and passenger doors respectively. Bulb seals are commonly found in locations where build variations cause significant variability in door gap widths. Figure 1(a) shows the locations where bulb seals are typically used. A sketch of one type of primary bulb seal assembly is shown in Figure 1(b). The bulb seals are often made of foamed rubber so that they can readily adapt to different mating surfaces and door clearances.

Sound transmitted through weather sealing systems may contribute significantly to interior noise in automobiles [1]. In cases where the seals do not perfectly block the flow through the gaps, intense aspiration noise can be produced. Great care is usually taken to ensure that this problem is avoided. In absence of aspiration, the transmission of sound through elastomeric sealing systems is mostly structural. Seal wall vibrations are induced by unsteady pressures produced by impinging sound waves from the exterior of the vehicle, or by turbulent flows over the vehicle body.

Some aspects of sound transmission through bulb seals are analogous to sound transmission through rectangular slots in walls of finite depth. The only difference is the

0022-460X/02/$35.00

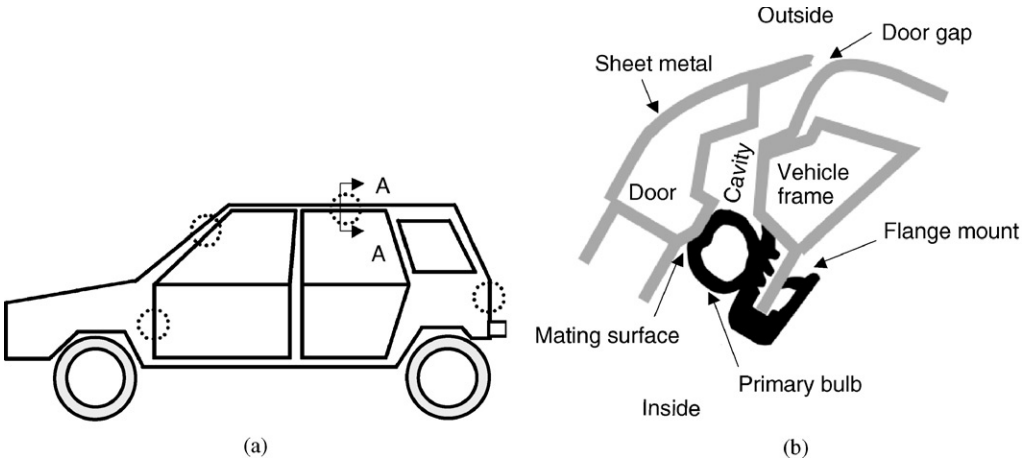

Figure 1. (a) Locations (inside dotted circles) where bulb seals are used in road vehicles; (b) cross-section (A-A) of a typical seal in host environment.

additional blockage provided by the bulb seal. Other aspects are analogous to the well-known problem of sound transmission through panels. There is a vast literature on the latter problem (for example reference [2]), and relatively sparser information about the former one. Some work has been directed towards sound transmission through circular holes, and elongated slits. Empty slots of circular and rectangular shapes, for example, were investigated by Gomperts [3]. Sound transmission through circular and rectangular slots of finite depths was studied using a reverberation room method by Wilson and Soroka [4]. In the same study, a model was developed for the three-dimensional radiated waves on the source and receiver sides and the standing plane wave inside the slot. It was found that rectangular slots could be successfully represented using equivalent circular holes over a wide range of aspect ratios.

The acoustic sealing of holes and slits in walls was investigated by Mechel [5]. The sound transmitted through circular holes and through long slits in a wall of finite thickness was computed analytically. Wall openings filled with porous absorbing materials and sealed using plastic sealing layers were considered, and the effects of sealing materials on sound transmission loss predictions were investigated. The sound transmission loss was influenced significantly by the sealing materials.

Experiments to determine the sound transmission loss of circular and slit-shaped apertures were conducted by Oldham and Zhao [6]. Sound intensity measurements were performed to measure the transmitted acoustic power. The aperture was assumed to act as a point sound source or a semi-cylindrical sound source. The approximate models by Gomperts [3] were found to be in good agreement with measured sound transmission loss values.

The sound insulation of building doors was investigated experimentally by Hongisto [7], and Hongisto *et al.* [8]. Two separate transmission paths were identified: structural transmission through a door panel and airborne transmission through slits. It was found that the choice of sealing material influences the sound transmission loss of the door significantly within specific frequency bands.

The prediction of sound transmission through sealing systems has been a topic of interest to the automobile industry for the last several years. Gur and Morman [9] used a finite element (FE) analysis method to determine the sound transmission loss of door seals. This method allows the effects of seal geometry, cavity shape, and seal material properties

to be considered. Strumolo [10] used simplified models to estimate seal noise generation in software packages for the prediction of interior aerodynamic noise. In these models, the sound transmitted through side-glass windows and seals are treated as the primary aerodynamic noise sources.

Seals are usually considered acoustically transparent (i.e., with a zero sound transmission loss) at frequencies in the vicinity of a "critical" frequency. The noise from window seals is then reportedly comparable in level to the broadband noise generated from window panel vibrations at that frequency. Buchheim *et al.* [11] determined the contribution of sound transmitted through door seals on vehicle interior noise. Aerodynamic interior noise was investigated by blocking the door seals with thin tape to effectively reduce the sound transmitted through the door seals. The A-weighted interior pressure level was measured at the driver's left ear using a full-size vehicle in an acoustically treated wind tunnel with and without the seals taped. The difference at a wind tunnel flow speed of 180 km/h in the 3150 Hz one-third octave band was approximately 10 dB. At low frequencies, there was little or no change. Although this test did not allow the contribution of specific seal segments to be estimated, it did indicate that door seals are important aeroacoustic noise sources. More recently, Her *et al.* [12] performed similar tests by taping the door seals and glass edges. The effect on the interior noise was greatest in the frequency range from 700 Hz to 2 kHz, where the levels were reduced by 4–6 dB for a wind tunnel flow speed of 129 km/h.

A lumped element, two-degrees-of-freedom model of a bulb sealing system was proposed by Mongeau and Danforth [13]. Predictions from this model were compared to measured sound transmission loss values. Two different excitation methods were considered, acoustic and aerodynamic. Both excitation methods yielded similar results for the sound transmission loss. The lumped element model showed promise as a design tool, but required the adjustment of the lumped parameter values to obtain reasonable agreement with experimental data. A laboratory method was developed to evaluate the sound transmission characteristics of road vehicle body seals by Mongeau *et al.* [14]. The performance of various seal designs was compared. Systematic design optimization methods were described by Mongeau *et al.* [15]. These earlier studies [13-15] provided the motivation for the present investigation.

The objective of the present investigation was to further investigate the performance of bulb seals as sound barriers. Preliminary results have appeared previously in a condensed form [16, 17]. Experiments were performed to measure the sound transmission characteristics, and the vibrational response of one bulb seal specimen. An FE-model for prediction of the sound transmission loss was developed. Various simplified geometries for the bulb seal models were first considered. A "dual-membrane" configuration was used for the verification of the numerical procedures. A rectangular geometry was then investigated to determine the effects of structural coupling between air-exposed seal membranes. Finally, the actual seal geometry was considered for comparisons with experimental results. The numerical analysis methods described in this paper offer the potential to perform seal design optimization studies in a short period of time, and at relatively low cost compared with experimental techniques.

2. EXPERIMENTAL METHODS

2.1. DESCRIPTION OF THE ELASTOMERIC BULB SEAL

The geometry of the seal considered is shown in Figure 2(a). In its uncompressed state, the seal possessed a height $D_0 = 14{\cdot}2$ mm, an external bulb diameter of approximately

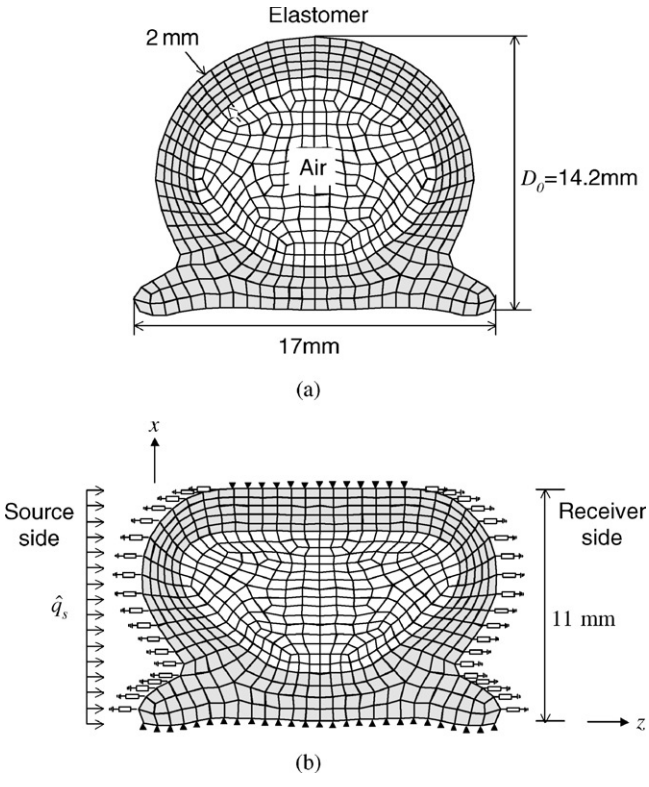

Figure 2. (a) FE-model of the bulb seal under investigation; (b) deformed shape of the bulb seal ($CR = 22\%$) and boundary conditions used in the dynamic analysis.

14 mm, a base width of 17 mm, and an average wall thickness of 2 mm.The seal was made of a foamed ethylene-propylene-diene (EPDM) rubber. The EPDM foam had the following physical constants: material density, $\rho_s = 370\,\text{kg/m}^3$; the Poisson's ratio, $v = 0{\cdot}4$; the loss factor, $\eta = 0{\cdot}16$. Table 1 shows the uniaxial compressive stress–strain data for the material. The seal material is relatively compliant, e.g., from the stress–strain data shown in Table 1, the nominal (unstressed) stiffness of the seal material is 2·3 MPa.

2.2. EXPERIMENTAL APPARATUS

The measurements of the sound transmission characteristics were performed using a reverberation room method. The reverberation room measured $7{\cdot}6 \times 6{\cdot}1 \times 5{\cdot}5\,\text{m}^3$, and featured a $1{\cdot}22 \times 1{\cdot}22\,\text{m}^2$ square wall aperture hosting structures under test. The experimental apparatus is shown in Figures 3(a) and (b). The aluminum test fixture was designed to host 24·8 cm long seal samples. Both ends of the samples were immersed in grease-filled cavities to minimize flanking sound transmission and leakage. The fixture walls were movable, allowing the seal height to be varied through the use of a micrometer. Bulb seal specimens were installed between two rigid blocks: a steel-mating block and an aluminum-hosting block. The base of the bulb seal was fixed to the hosting block using an adhesive. Figure 4 shows a picture of the actual test fixture as viewed from the reverberation room. Efforts were made to minimize any flanking sound transmission

TABLE 1

Stress–strain relationship for the seal material

Engineering strain	Engineering stress (MPa)
0·03	0·07
−0·03	−0·07
−0·09	−0·17
−0·15	−0·34
−0·21	−0·56

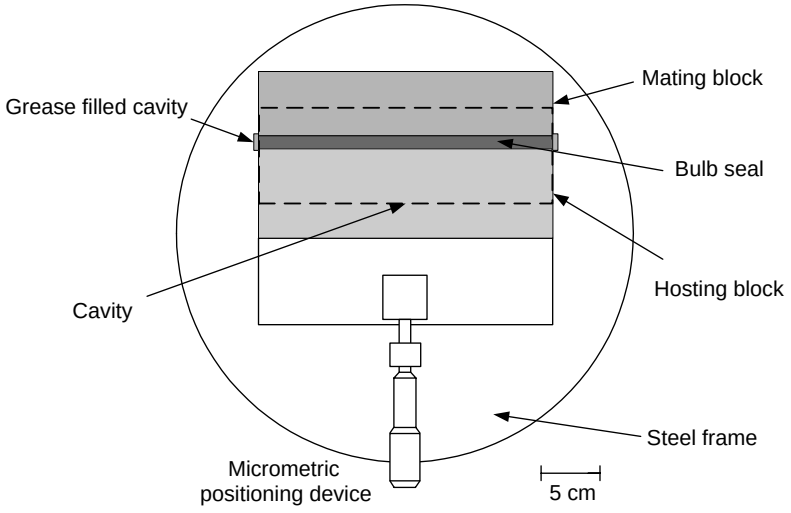

(a)

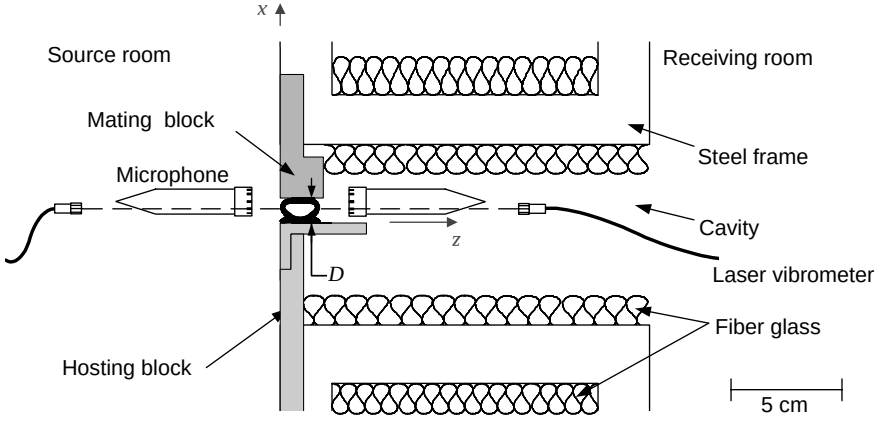

(b)

Figure 3. Description of the experimental set-up used for the experiments, drawn to scale. (a) Front view; (b) side view of the fixture.

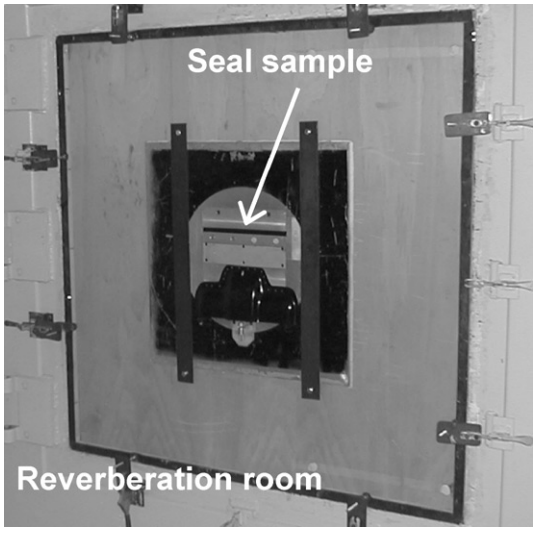

Figure 4. Picture of the seal fixture, taken in the reverberation room.

through the wall aperture to the receiver side of the test apparatus by surrounding the test fixture with a well-sealed double-panel wall, also shown in Figure 3.

Two loudspeakers were used as sound sources for the generation of a nearly diffuse sound field within the reverberation room. Sound intensity measurements on the receiver side were performed inside a cavity within the fixture. The interior surfaces of the cavity walls were treated with sound-absorbing materials to reduce potential acoustic cavity resonance effects.

2.3. SURFACE ACOUSTIC INTENSITY MEASUREMENTS

Surface intensity [18] measurements were performed. The transverse velocity along the seal wall was measured using a Polytec laser vibrometer, equipped with a controller processor model OFV-3000, and a fiber optic laser interferometer model OFV-511 [19]. This vibrometer has a resolution of 0·5 μm/s and a maximum signal bandwidth of 35 kHz. The vibration measurements were performed at evenly spaced locations along the seal height at the center of the seal sample. The sound pressure was synchronously measured near the vibration measurement locations using one 12·7 mm condenser microphone.

The effective spatially averaged velocity of the seal on the source side was estimated as

$$\hat{v}_{se} = \frac{1}{N}\sum_{k=1}^{N} \hat{v}_{sk}, \tag{1}$$

where N is the number of velocity measurement locations on one side of the bulb seal, $\hat{v}_{se}$ is the effective velocity of the seal wall, and $\hat{v}_{sk}$ is the measured complex velocity of the seal wall at the kth measurement point. The phase reference was the complex pressure $\hat{p}_s$ measured on the source side near the velocity measurement point. All velocity components are in the z direction only. The index s indicates source side measurements. The corresponding specific acoustic impedance ($\hat{Z}_s$) was defined as

$$\hat{Z}_s = \frac{\hat{p}_s}{\hat{v}_{se}}, \tag{2}$$

where the usual complex notation is used, i.e. $v(t) = \mathrm{Re}\{\hat{v}(\omega)\mathrm{e}^{\mathrm{i}\omega t}\}$.

Similarly, the effective velocity and the specific acoustic impedance on the receiver side were determined using the equations

$$\hat{v}_{te} = \frac{1}{N}\sum_{k=1}^{N} \hat{v}_{tk}, \qquad \hat{Z}_t = \frac{\hat{p}_t}{\hat{v}_{te}}, \tag{3,4}$$

where $\hat{v}_{te}$ is the effective velocity, $\hat{v}_{tk}$ is the complex velocity at the kth measurement point with reference to $\hat{p}_t$, the complex pressure on the receiver side near the velocity measurement point, and $\hat{Z}_t$ is the specific acoustic impedance. The index t indicates the receiver side measurements or transmitted quantities.

The acoustic intensity absorbed by the bulb seal, I_s, was calculated from the measured quantities using

$$I_s = \mathrm{Re}\{\hat{p}_s \hat{v}_{se}^*\}, \tag{5}$$

where $\hat{v}_{se}^*$ is the complex conjugate of $\hat{v}_{se}$. The absorbed intensity is related to the incident intensity (I_i) and the reflected intensity (I_r) through the energy balance

$$I_i - I_r = I_s. \tag{6}$$

A fraction of the absorbed intensity, the dissipated intensityI_d, accounts for dissipation into heat due to material damping. The remaining part of the absorbed intensity is transmitted to the receiver side. The absorbed intensity is related to the dissipated and the transmitted intensity, I_t, such that $I_s = I_d + I_t$, as illustrated in Figure 5. The transmitted intensity, I_t, was calculated from the measured velocity and pressure on the receiver side using

$$I_t = \mathrm{Re}\{\hat{p}_t \hat{v}_{te}^*\}. \tag{7}$$

The measured sound transmission loss of the bulb seal, R_{TL}, is defined as [2]

$$R_{TL} = 10 \log\left(\frac{I_i}{I_t}\right). \tag{8}$$

The incident intensity was calculated assuming a diffuse sound field in the reverberation room using the effective incident intensity [20] defined as

$$I_i = \frac{|\hat{p}_m|^2}{4\rho c}, \tag{9}$$

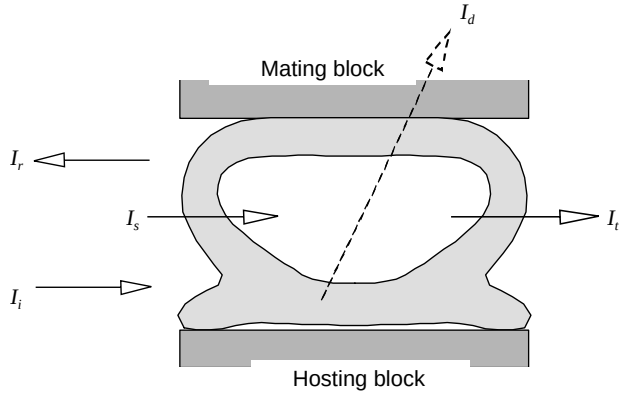

Figure 5. The sound transmission through bulb seals. Illustration of energy balance.

where $\hat{p}_m$ is the mean sound pressure on the source side, ρ is the density of air ($1{\cdot}21\,\mathrm{kg/m^3}$), and c is the speed of sound in air (343 m/s). The measured sound pressure on the source side, $\hat{p}_s$, may be higher than the mean sound pressure, but lower than the blocked sound pressure in magnitude due to the compliance of the bulb seal. It is well known that the blocked pressure measured on a rigid wall in a reverberant room is approximately 3 dB higher than the value measured in the reverberant sound field away from rigid surfaces (without any direct field from the sound source) [3]. In this study, it was assumed that the measured sound pressure on the source side was identical to the mean sound pressure in the reverberation room ($\hat{p}_m = \hat{p}_s$). This assumption yielded better agreements between experimental data and numerical simulations than assuming the measured sound pressure on the source side as the blocked pressure.

3. NUMERICAL MODELS

3.1. METHODS

A numerical analysis of sound transmission through the bulb seals was performed using the FE-method. This approach allows the complex geometry of the bulb seal, specific constitutive equations for the foamed EPDM rubber, and arbitrary acoustic boundary conditions to be taken into consideration. In all simulations, the seal material and the air trapped in the bulb were modelled using four-node bilinear elements under a plane strain assumption. The seal material was treated as an isotropic non-linear viscoelastic solid. Air was modelled by the use of acoustic elements, which possess acoustic pressure as the sole degree of freedom. The finite element mesh used in the analysis of the seal is depicted in Figure 2 for undeformed and deformed configurations.

Foamed rubbers commonly used in sealing systems are generally treated as materials with fading memory [21]. Thus, when constrained to a state of deformation constant for a time period sufficient to allow the applied forces to relax, the final state of the elastomer mechanical properties depends only on the current state of the deformation [22]. If the amplitude of the applied vibration due to the acoustic loading is sufficiently small, then the equations describing the dynamic response of the seal material can be linearized.

In the computational analysis, the seal shape after compression by the mating surface was first calculated using a quasi-static model, i.e., for boundary conditions independent of time. This step represents the deformation of the seal which in the actual installation would be caused by door closure. It was initially postulated that the sound transmission properties of seals might depend upon the stress state in the seal after compression. The computational model was designed to allow this possible effect to be taken into consideration. Following the static analysis, a linear perturbation analysis was performed. A steady state dynamic linear perturbation procedure based on the actual physical degrees of freedom was used to calculate the frequency-dependent response of the model and to predict the sound transmission characteristics of the bulb seal. All computations were performed using the commercially available software ABAQUS [23].

The interface between the seal material and the entrapped air was modelled using acoustic coupling elements. These elements impose equal accelerations in the direction normal to the interface of adjacent elements on both sides of the interface. They allow structural–acoustic interactions between acoustic gas pulsations in the air cavity and seal wall vibrations to be accounted for.

A wall pressure excitation was applied on the source side of the seal. The partition of sound waves into an incident and a reflected component was done *a posteriori*. This

eliminated the need for surrounding the bulb seal by acoustical elements, thus reducing computational costs.

Impedance boundary conditions were imposed on the exterior walls of the seals. These boundary conditions allow the acoustic loading effects on the seal vibration to be accounted for. Assuming plane-travelling waves on both sides of the seal (with no reflections), the acoustic loading is purely dissipative, equal to the impedance of planar propagating sound waves in the direction of wave propagation. Damping elements aligned in the direction of wave propagation were used to account for such energy dissipation, see Figure 2(b). As an illustration of this method, consider a limp panel of mass per unit area m excited by a distributed force, as shown in Figures 6(a) and 6(b). For the limp panel in Figure 6(a), surrounded by air of density, ρ, the equation of motion is

$$2\hat{p}_i = 2\mathrm{i}\omega\rho c\hat{\xi} - m\omega^2\hat{\xi}, \tag{10}$$

with $\hat{\xi}$ the complex panel displacement and $\hat{p}_i$ the incident complex acoustic pressure. The reflected and transmitted waves are taken into account in equation (10). The equation of motion for the limp panel depicted in Figure 6(b) is

$$\hat{q}_s = 2\mathrm{i}\omega b\hat{\xi} - m\omega^2\hat{\xi}, \tag{11}$$

where $\hat{q}_s$ is a complex distributed load and b is the damping coefficient accounting for the dissipative air loading effects ($b = \rho c$). From the analogy between equations (10) and (11), the incident pressure is exactly half the excitation pressure. This conclusion can be easily extended to other higher order systems. Distributed loads were applied to the source side of the bulb seal. The sound transmission loss of the bulb seal, $R_{TL,F}$, was calculated as

$$R_{TL,F} = 20\log\left|\frac{\hat{q}_s}{2\rho c\hat{v}_{te,F}}\right|, \qquad \hat{v}_{te,F} = \frac{1}{D}\int_D \hat{v}_{t,F}(z)\cdot e_z\,\mathrm{d}z, \tag{12, 13}$$

where e_z is the unit vector along the z direction (Figure 3), $\hat{v}_{t,F}(z)$ is the computed complex particle velocity at the surface of the bulb seal on the receiver side, $\hat{v}_{te,F}$ is the complex effective value, and D is the seal height in the compressed state. Similarly, on the source side, the complex effective velocity was calculated using

$$\hat{v}_{se,F} = \frac{1}{D}\int_D \hat{v}_{s,F}(z)\cdot e_z\,\mathrm{d}z. \tag{14}$$

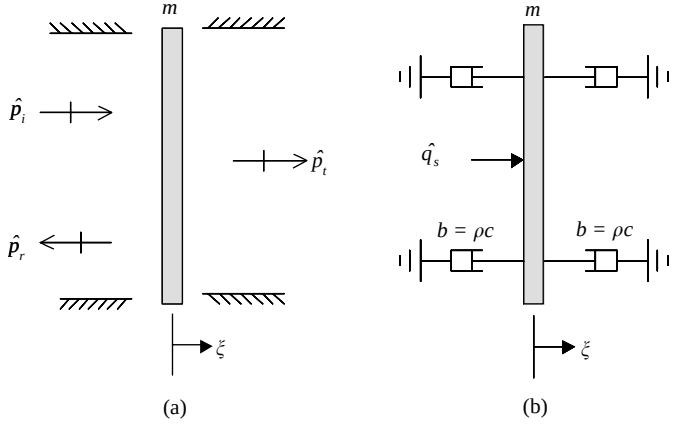

Figure 6. A simple example (a limp panel of mass per unit area m) of substitution of an acoustic pressure load with a mechanical distributed load: (a) acoustic pressure excitation of the limp panel surrounded by the air; (b) the limp panel excited by the mechanical distributed load (air loading effects are replaced by equivalent dashpots).

The intensity absorbed by the seal on the source side was calculated using

$$I_{s,F} = \mathrm{Re}\left\{\hat{q}_s \hat{v}^*_{se,F}\right\}. \tag{15}$$

Assuming plane-travelling waves on the receiver side of the seal, the transmitted intensity was finally calculated using

$$I_{t,F} = \rho c \left|\hat{v}_{te,F}\right|^2. \tag{16}$$

3.2. VERIFICATION OF THE COMPUTATIONAL METHOD

To verify the FE-model, the case of two structurally independent membranes separated by an air gap was treated, as illustrated schematically in Figure 7(a). The seal membranes were assumed to be free to move along the z direction, the direction of wave propagation. Friction forces on the upper and lower boundaries of the seal were neglected. Within the air cavity, the sound field is comprised of incident and reflected waves. The complex amplitudes of the reflected and transmitted monochromatic planar pressure waves are $\hat{p}_r$ and $\hat{p}_t$ respectively. Longitudinal planar waves are assumed to be present within the seal material as well, with complex amplitudes for the incident and reflected waves within each membrane.

A transfer function matrix method was used to calculate the sound transmission loss. In the transfer function matrix method, the imposition of continuity of pressure and

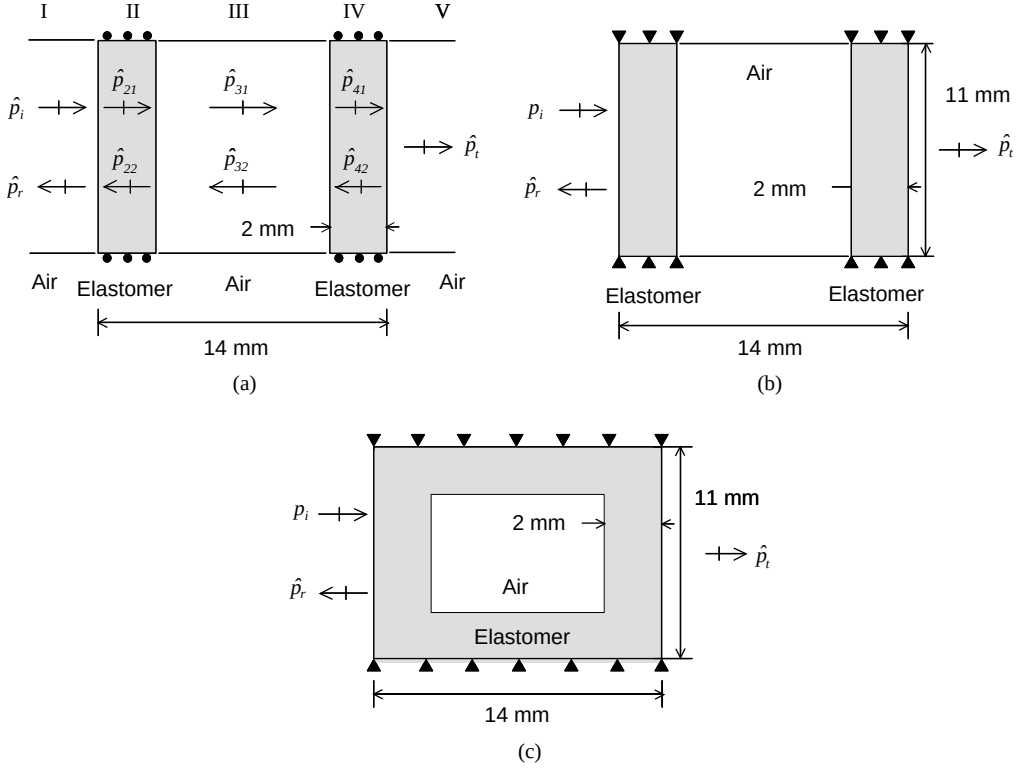

Figure 7. Simplified geometric models of bulb seals: (a) idealized dual-membrane model; (b) dual-membrane model with fixed boundary conditions at their ends; (c) rectangular model.

transverse velocity of the travelling wave fields at each boundary yields relationships between the incident and the transmitted complex pressure in each layer. For the present system consisting of a total of five layers the transfer function matrix has the form of an 8×8 matrix. The final relationship between the incident, the transmitted, and the reflected pressure amplitudes is

$$\begin{bmatrix} -1 & 1 & 1 & 0 & 0 & 0 & 0 & 0 \\ r_{2,1} & 1 & -1 & 0 & 0 & 0 & 0 & 0 \\ 0 & e^{-ik_2 d_1} & e^{ik_2 d_1} & -1 & -1 & 0 & 0 & 0 \\ 0 & r_{3,2}e^{-ik_2 d_1} & -r_{3,2}e^{ik_2 d_1} & -1 & 1 & 0 & 0 & 0 \\ 0 & 0 & 0 & e^{-ik_3 L} & e^{ik_3 L} & -1 & -1 & 0 \\ 0 & 0 & 0 & r_{4,3}e^{-ik_3 L} & -r_{4,3}e^{ik_3 L} & -1 & 1 & 0 \\ 0 & 0 & 0 & 0 & 0 & e^{-ik_4 d_2} & e^{ik_4 d_2} & -1 \\ 0 & 0 & 0 & 0 & 0 & r_{5,4}e^{-ik_4 d_2} & -r_{5,4}e^{ik_4 d_2} & -1 \end{bmatrix} \begin{bmatrix} \hat{p}_r \\ \hat{p}_{21} \\ \hat{p}_{22} \\ \hat{p}_{31} \\ \hat{p}_{32} \\ \hat{p}_{41} \\ \hat{p}_{42} \\ \hat{p}_t \end{bmatrix} = \begin{bmatrix} 1 \\ r_{2,1} \\ 0 \\ 0 \\ 0 \\ 0 \\ 0 \\ 0 \end{bmatrix} \hat{p}_i, \tag{17}$$

where $r_{j+1,j} = \rho_{j+1} c_{Lj+1} / \rho_j c_{Lj}$ is the ratio of the specific acoustic impedances of two adjacent layers j and $j+1$, $k_j = \omega / c_{Lj}$ is the wavenumber for each layer, d_1 and d_2 are the wall thicknesses, L is the separation distance between membranes, and $\hat{p}_{j1}$ and $\hat{p}_{j2}$ are the assumed complex pressures. The wavenumber in the solid was assumed to be real, i.e., the dissipation due to material damping was neglected. The wave speed inside the seal layers, $c_{L,}$ was obtained using [24]

$$c_L = \sqrt{\frac{E(1-v)}{\rho_s(1+v)(1-2v)}}. \tag{18}$$

This matrix system of equations was solved to obtain the complex pressure coefficients from which the sound transmission loss was calculated.

An FE-model was also developed for the dual-membrane seal model of Figure 7(a). A comparison between the sound transmission loss of the dual-membrane seal model computed using the transfer function matrix method and the FE-method is shown in Figure 8 for the case of $d_1 = d_2 = 2\,\text{mm}$ and $L = 10\,\text{mm}$. Material damping was neglected and no initial strain was prescribed. A good agreement between the numerical and the analytical model predictions was obtained. Since the transfer function matrix method is expected to yield accurate predictions for the set of assumptions made in the analysis, this result demonstrates the accuracy of the numerical model. In agreement with results by Gur and Morman [9], there is a resonance frequency where R_{TL} become zero. This frequency corresponds to the mass–air–mass resonance frequency of the seal. At this resonance frequency, the seal behaves as two masses connected with a spring element accounting for effects of the compliance of the air trapped within the bulb. For the dual-membrane seal model of Figure 7(a), the mass–air–mass resonance frequency, f_0, is [2]:

$$f_0 = \frac{1}{2\pi}\sqrt{\left(\frac{\rho c^2}{L}\right)\left(\frac{d_1 + d_2}{\rho_s d_1 d_2}\right)}. \tag{19}$$

The calculated resonance frequency was 903 Hz which is very close to the frequency value where $R_{TL,F}$ is zero in Figure 8. It may be noted that the resonance frequency for the simple dual-membrane model is considerably lower than the value measured for the actual seal (shown later), despite the fact that the dimensions and the material properties were similar.

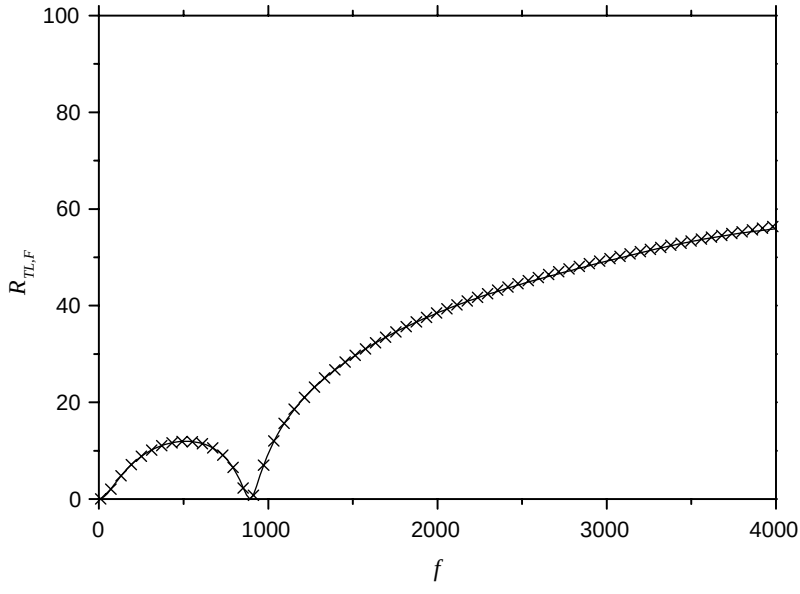

Figure 8. Sound transmission loss predictions for a simplified dual-membrane seal model: ×, transfer function matrix method; ———, FE-analysis.

Other models were created to elucidate the general behavior of the system. One model was a dual-membrane model such as that described above, but with fixed boundaries as shown in Figure 7(b). A slightly more complex model, depicted in Figure 7(c), consisted of a rectangular seal. Results obtained from these models were subsequently compared to those obtained for models accounting for the actual seal geometry.

A convergence study was performed using the rectangular seal model. A mesh with a uniform element size was used for both the gas and the solid. The dependence of the predicted sound transmission loss on the element size in the wave propagation direction, h, was investigated. In general, the convergence of the solution depends on the number of internodal intervals within one acoustic wavelength at the highest frequency of interest ($f = 4000$ Hz, here). For the present material parameters, the wavelength in the solid is shorter than that in the air; thus the ratio $c_L/(hf)$ characterizes the spatial resolution of the finite element mesh. Figure 9 shows the effects of element size on the predicted sound transmission loss for $c_L/(hf) = 20{\cdot}5, 41, 82$ respectively. In the present study, the predicted sound transmission loss was mostly influenced by the stress concentration factor. For the element sizes exercised, the predicted sound transmission loss varied with the element size only at high frequencies. For the frequency range of interest, the sound transmission loss was essentially independent of the element size for $c_L/(hf) > 41$.

3.3. MODELS FOR ACTUAL SEAL GEOMETRY

The numerical procedures for the actual seal geometry started with the undeformed bulb seal and the deformed air shape. First, a static deformation of the bulb seal was imposed (a static analysis was performed). The interior air cavity pressure was ignored in the static analysis. The acoustic–structure interactions were enforced between the seal and the entrapped air after the static analysis. Then, dynamic simulations to investigate the sound transmission through the bulb seal were performed. This numerical procedure for

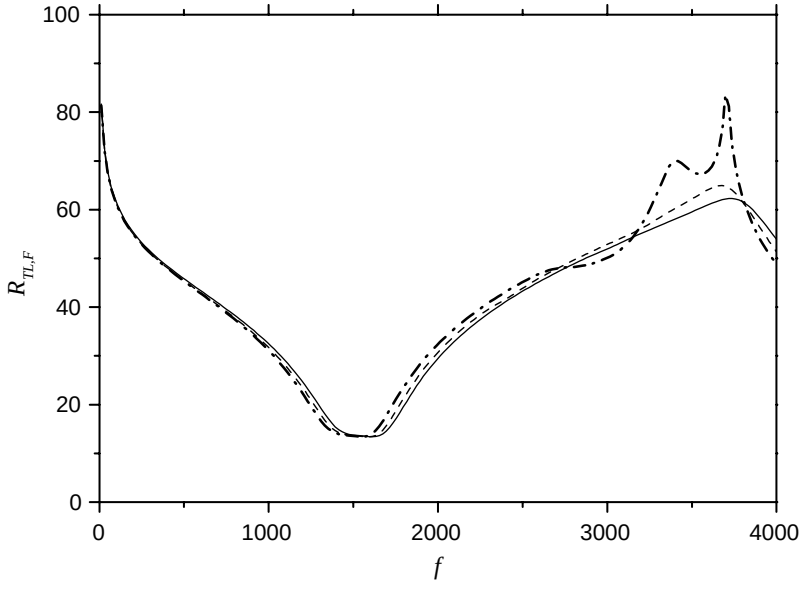

Figure 9. Variation of the predicted sound transmission loss of the rectangular seal model with element size. Value of $c_L/(hf)$: –·–·–·–, 21·5; – – – – –, 41; ———, 82.

the static seal loading was developed to avoid unrealistic pressure build up in the seal cavity upon static loading.

In the dynamic analysis, the nodes in contact with the mating block on the boundary were fixed. The contact area between the mating block and the bulb seal rapidly increases as the seal compression is increased. Frictional forces are present between the bulb seal and the mating block. One important issue is to determine whether the two surfaces may slip against each other. This can be surmised to a certain extent from the experimental data that will be shown later. In the case where there is no contact between the seal and the mating block, the measured sound transmission loss is low compared to that measured for the case where the seal is in contact with the mating block, especially at frequencies below 1 kHz. This behavior is typical of a fixed boundary condition, for which the sound transmission loss tends towards infinity as the frequency tends towards zero (a fixed boundary implies an infinitely large stiffness). The low-frequency limit of the experimental data suggests a fixed boundary, implying no relative motion between the seal and the mating block. Fixing the nodes in contact with the wall, however, may overconstrain the motion of the solid walls near the edges of the contact patch. These areas could perhaps lift slightly as the walls vibrate in reality.

4. RESULTS

4.1. INFLUENCE OF GEOMETRY ON MODEL PREDICTIONS

Figure 10 shows a comparison of the predicted sound transmission loss for three different models: (1) the dual-membrane model with fixed boundaries, Figure 7(b); (2) the rectangular seal model, Figure 7(c); and (3) the model with actual seal geometry, Figure 2(b). The dynamic analysis was performed without initial static deformation for all of these three models. Identical wall thicknesses, material properties, and seal heights were used for all three models. The results, shown in Figure 10, reveal interesting trends in the

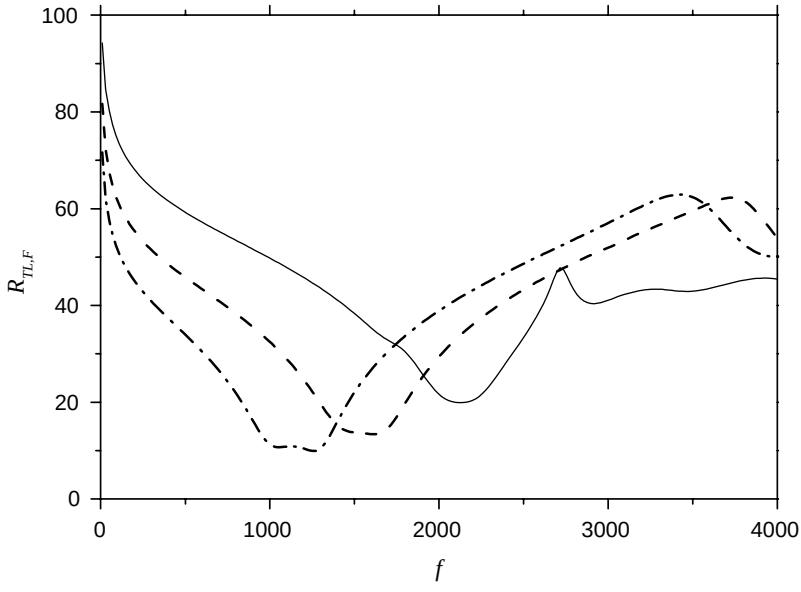

Figure 10. Comparison between the predicted sound transmission loss of the bulb seal using three different models: –·–·–, dual-membrane model with membranes fixed on bottom and top; – – – – –, rectangular model; ———, actual seal geometry model.

predicted resonance frequency. The dual-membrane model yields the lowest resonance frequency. The predicted resonance frequency for the rectangular seal model is approximately 500 Hz higher than that for the dual-membrane model. This effect is a result of the stiffening effects of the side walls which are fixed to the rigid boundaries and provide structural coupling between the membranes. The specific acoustic impedance of the air gap between membranes is much smaller than that of the seal material. Consequently, the equivalent specific impedance of the rectangular model is greater than that of the dual-membrane model. The predicted resonance frequency for the real seal geometry model is yet greater than that for the other two models. This trend is presumably due to the stiffening effects from increased contacting area. These results suggest that details of the actual seal geometry have a strong impact on the mass–air–mass resonance "dip" in the sound transmission loss.

4.2. MEASURED SOUND TRANSMISSION LOSS OF THE BULB SEAL

Two different approaches were followed to measure the acoustic intensities defined in equations (5) and (7). The first approach assumed plane-travelling waves. This is inaccurate due to the presence of sound wave reflections within the fixture cavity. The second approach made direct use of the measured specific acoustic impedance.

The effects of seal compression on the sound transmission loss were determined first. The seal surface velocity was measured at one location ($N = 1$). The surface velocity was assumed to be uniform along the height of the seal on the receiver side. Plane wave sound propagation on the receiver side of the seal was assumed for the determination of the transmitted sound intensity from experimental data (assuming $\hat{Z}_t = \rho c$). Possible resonance phenomena in the fixture cavity were thus not considered for in this case.

Figure 11 shows the measured bulb seal sound transmission loss for four different seal compression ratios as a function of frequency. The compression ratio was defined as

$$CR = \frac{D_0 - D}{D_0} \times 100\%. \tag{20}$$

The graphs of sound transmission loss versus frequency feature a pronounced dip, with a minimum between 1500 and 2500 Hz. The frequency of this minimum increases as the compression ratio is increased. The presence of minimum in R_{TL} is typical of double wall sound barrier constructions, as mentioned previously. The frequency of minimal sound transmission loss corresponds to the mass–air–mass resonance frequency. The measured resonance frequencies are greater than the value that was calculated using equation (19) due to the stiffening effects from the fixed boundaries of the seal, which was discussed in the previous section.

For negative values of the compression ratio, i.e., when the seal is not in contact with the mating surface, the sound transmission loss is comparatively smaller, especially at frequencies below 1 kHz. Such trend in the sound transmission loss behavior results from a resonance mode involving the rigid-body motion of both bulb seal membranes. This mode is greatly reduced when the seal is in contact with the wall, because friction forces then prevent the motion of the seal as a rigid body. It was identified through the analysis of the velocity signals, since the transmitted sound information alone does not allow the airborne leakage sound to be isolated from the transmitted sound unambiguously.

4.3. MEASURED SPECIFIC ACOUSTIC IMPEDANCE

A series of experiments was performed to investigate the specific acoustic impedance on both sides of the seal. The vibration of the seal wall was measured at eight locations

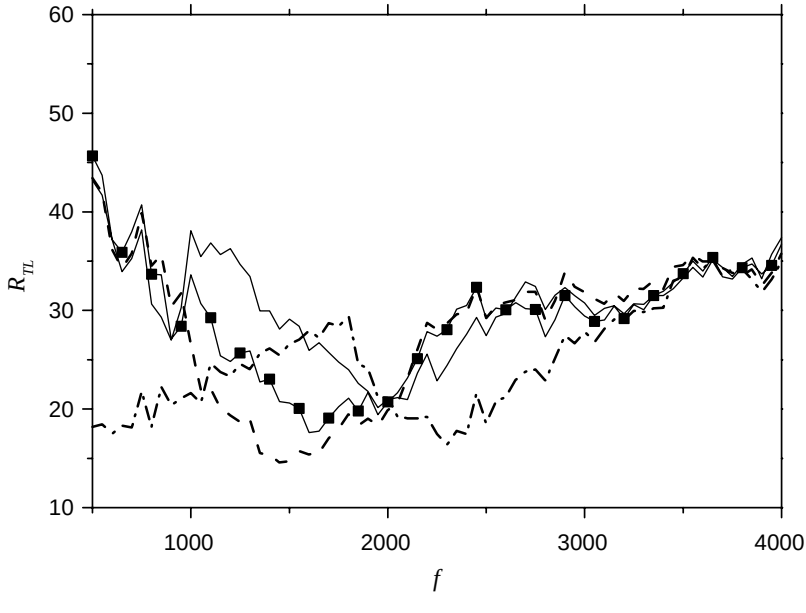

Figure 11. Measured sound transmission loss of the bulb seal using the plane-travelling wave assumption for different values of the compression ratio, *CR*: –·–·–, −5%; – – – –, 9·8%; —■—, 16·9%; ———, 22·5%.

($N = 8$). The measurement locations were aligned along the seal wall in the x direction and separated by a distance of 1 mm.

The specific acoustic impedance on the source side ($\hat{Z}_s$) is a function of the bulb seal mechanical impedance and loading effects from the surrounding air. The measured specific acoustic impedance on the receiver side ($\hat{Z}_t$) only includes loading effects from the surrounding air and the fixture cavity.

Figure 12(a) shows the measured specific acoustic impedance on the source side as a function of frequency. The real part of the measured specific impedance, the resistance, is indicative of the sound absorption coefficient of the bulb seal. The imaginary part of the measured specific impedance, or reactance, is a measure of the potential forces acting on the system. This quantity changes sign from negative to positive around 2300 Hz. The frequency at which the sign change of the reactance occurs corresponds to the seal resonance frequency. Again, the resonance frequency was found to increase with increasing compression ratio, a trend already observed in the previous sound transmission loss measurements (for which plane-travelling waves were assumed).

Figure 12(b) shows the impedance measured on the receiver side, a measure of acoustic loading effects, for two different compression ratios. Real parts and imaginary parts correspond to the resistance and the reactance respectively. These data were used for the impedance boundary condition imposed on this seal wall in the following numerical simulations. Large variations of the measured specific acoustic impedance can be observed in the frequency range between 500 and 2000 Hz (Figure 12). These variations may be an artifact induced by vibrations of the hosting block due to the compliance of its supports. In this frequency range, the coherence between the velocity and the sound pressure measured was less than 0·1. Nevertheless, the coherence was good around the resonance frequency. This suggests that the vibration of the hosting block may have created some flanking transmission, except around the mass–air–mass resonance region where transmission through the seal walls may have been predominant.

4.4. VIBRO-ACOUSTIC RESPONSE OF THE BULB SEAL

In subsequent results, predictions from the FE-model for the actual bulb seal geometry are discussed. The measured acoustic impedance (Figure 12(b)) was imposed as impedance boundary conditions on the receiver side. The impedance was imposed in the direction of the assumed travelling wave propagation (z direction) only. Figure 13 shows the effects of the imposed impedance boundary conditions. The acoustic loading effects were minimal, except around the resonance frequency region. The impact of the reactance was in particular negligibly small, and thus neglected in subsequent studies.

Figure 14 shows the absorbed (I_s) and the transmitted (I_t) sound intensity via the bulb seal measured for $CR = 16{\cdot}9\%$. The ratio of transmitted intensity to absorbed intensity does not exceed 10%, indicating that the major portion of the absorbed intensity is dissipated through material damping (into heat) rather than being transmitted as sound. This result confirms that the damping characteristics of the elastomer used to manufacture the bulb seal may play an important role in the sound barrier properties of the seal. Figure 14 also shows the predicted acoustic intensities from the numerical model. The intensity ratio from the numerical model was in reasonably good agreement with the measured value. The absorbed and transmitted acoustic intensity should be always positive. The negative values shown were attributed to measurement errors in the case of the experiments, and to numerical errors in the analytical model due to the small value of the

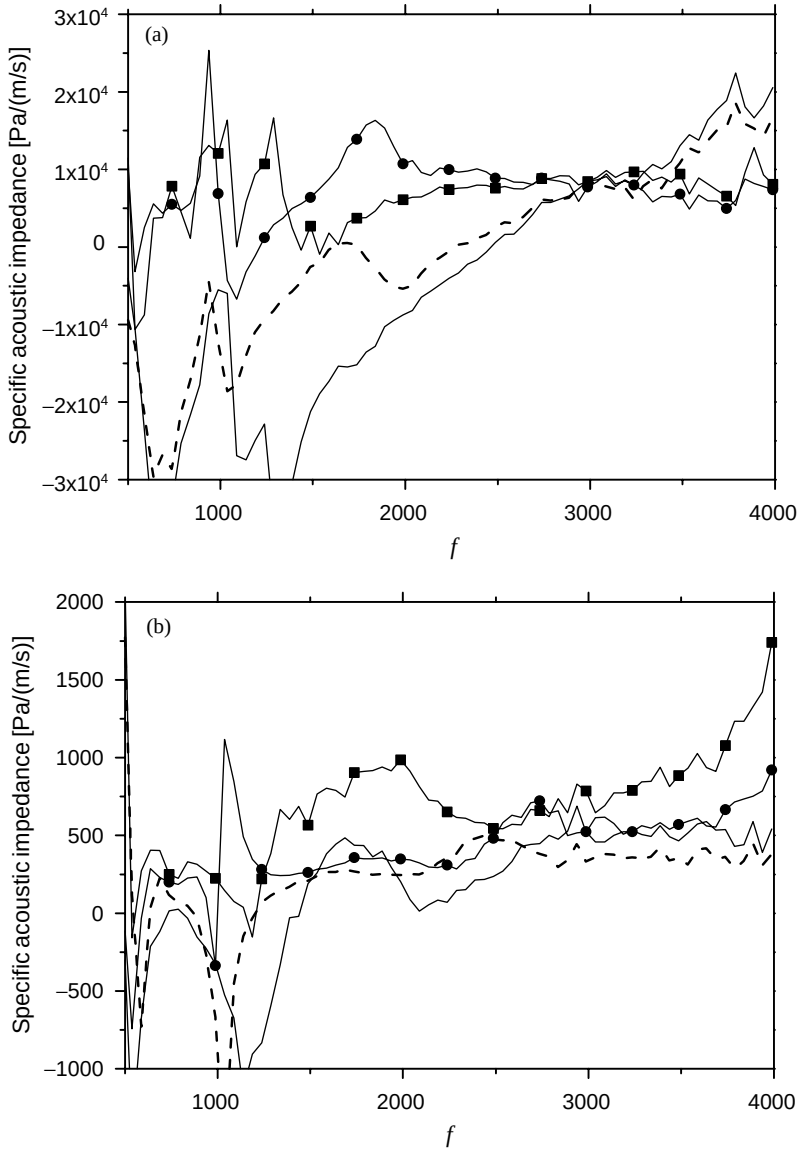

Figure 12. Specific acoustic impedance determined from surface acoustic intensity measurements on (a) the source side and (b) the receiver side. —■—, real part; ———, imaginary part for $CR = 22{\cdot}5\%$; —●—, real part; – – – – –, imaginary part for $CR = 16{\cdot}9\%$.

intensity in the case of the computations. Such errors occur especially at high frequencies where vibratory modes featuring bending waves dominated the seal response.

Figures 15(a) and 15(b) show the wall velocity spectral levels on the source side and on the receiver side, respectively, for two different compression ratios. The predictions are in good agreement with experimental data. The agreement is better on the source side than on the receiver side. As expected, the seal surface velocity level reaches a maximum around the resonance frequency. It should be noted that the local maximum around 1 kHz, a frequency at which the coherence was low, was believed to be a byproduct of the vibrations of the hosting block as mentioned previously.

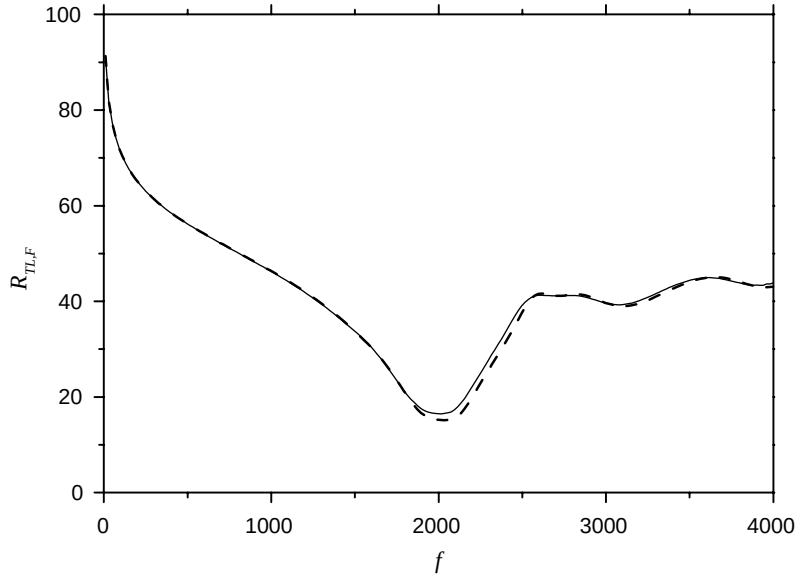

Figure 13. Effects of boundary conditions: ———, impedance boundary conditions imposed on the receiver side based on measured air loading effects; – – – – –, no impedance boundary conditions (i.e., neglecting air loading effects).

Figure 16 shows a comparison between the measured and predicted sound transmission loss. The measured results were calculated from the surface intensity data for $N = 8$. The general trend of the frequency dependence of the sound transmission loss was predicted well. The sound transmission loss reaches a minimum value between 1500 and 2500 Hz. A larger compression ratio causes the range of low sound transmission loss to be shifted to higher frequencies. The main discrepancies between numerical and experimental data arise in the resonance region where the sound transmission loss is underestimated by the numerical simulations by approximately 5 dB.

4.5. PARAMETRIC STUDY

The numerical model was finally used to investigate the effects of several bulb seal design parameters on the sound transmission loss. Figure 16 shows the effect of the seal compression ratio on the predicted sound transmission loss. An increase of the mass–air–mass resonance frequency is predicted as the compression ratio is increased. As the compression ratio is increased, the equivalent stiffness of the bulb seal is increased due to a change in geometry. The geometry change is also responsible for an increase in the contact area between the seal and the mating block. The increase in the compression ratio yields an increased sound transmission loss in the low-frequency region below resonance, a shift of the resonance region to higher frequencies, but has little impact on the sound transmission loss at frequencies above resonance.

During seal manufacturing, variations in rubber compounds and foaming parameters can result in changes in seal material properties. The FE-model was used to investigate the effect of the elastic modulus and the loss factor on the sound transmission loss. Figure 17(a) depicts the effect of the elastic modulus. Changes in elastic modulus cause substantial changes in the sound transmission loss below the mass–air–mass resonance frequency. This region corresponds to the stiffness-controlled region. Decreasing the seal

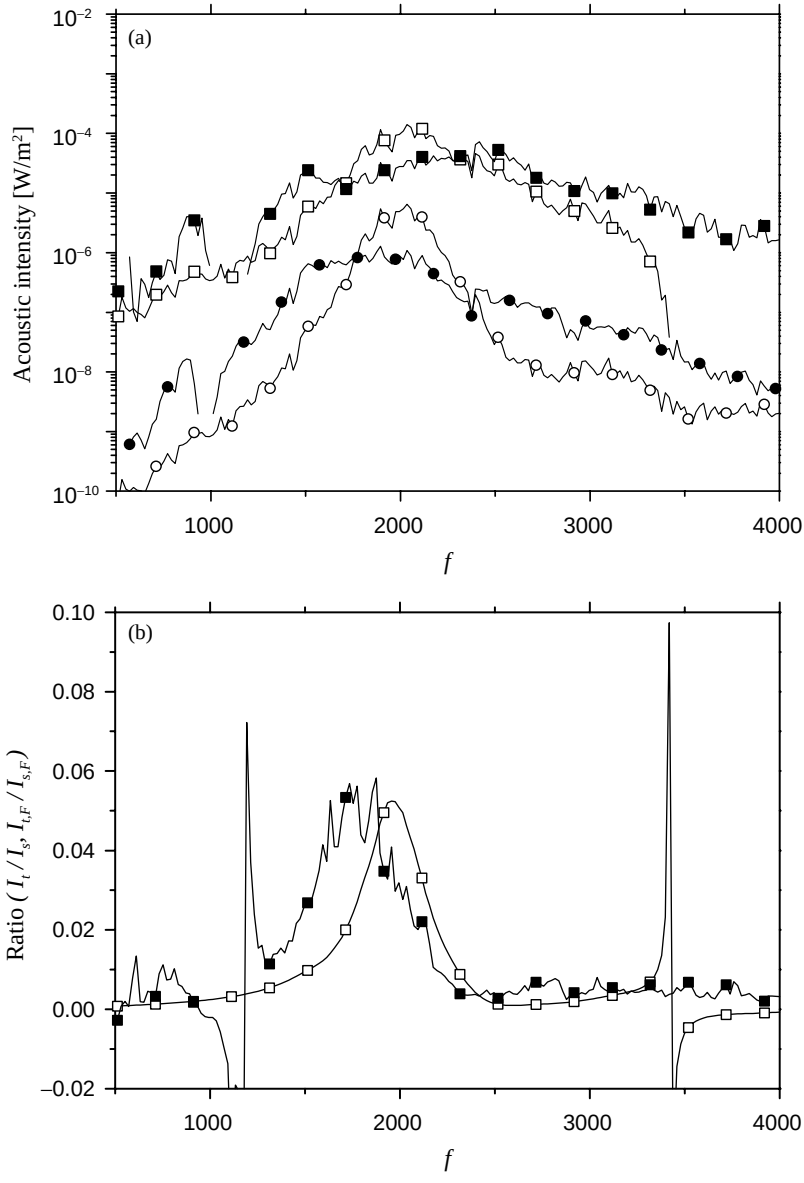

Figure 14. (a) Absorbed intensity from the diffuse sound field into the seal: —■—, measured; —□—, calculated, and transmitted intensity into the receiver side: —●—, measured; —○—, calculated and (b) their ratio (transmitted intensity/absorbed intensity): —■—, measured; —□—, calculated. $CR = 16{\cdot}9\%$.

material stiffness reduces the sound transmission loss in this region. Furthermore, a reduction of seal material stiffness is observed to lead to a reduction in resonance frequency. At frequencies above the mass–air–mass resonance frequency, i.e., in the mass-controlled region, the sound transmission loss did not depend strongly on the seal material stiffness. Figure 17(b) shows the effects of the loss factor of the seal material on the predicted sound transmission loss values. The loss factor affected the sound transmission loss mostly in the mass–air–mass resonance frequency region. Decreasing the loss factor leads to a decrease in the sound transmission loss. Changes in the loss factor also slightly

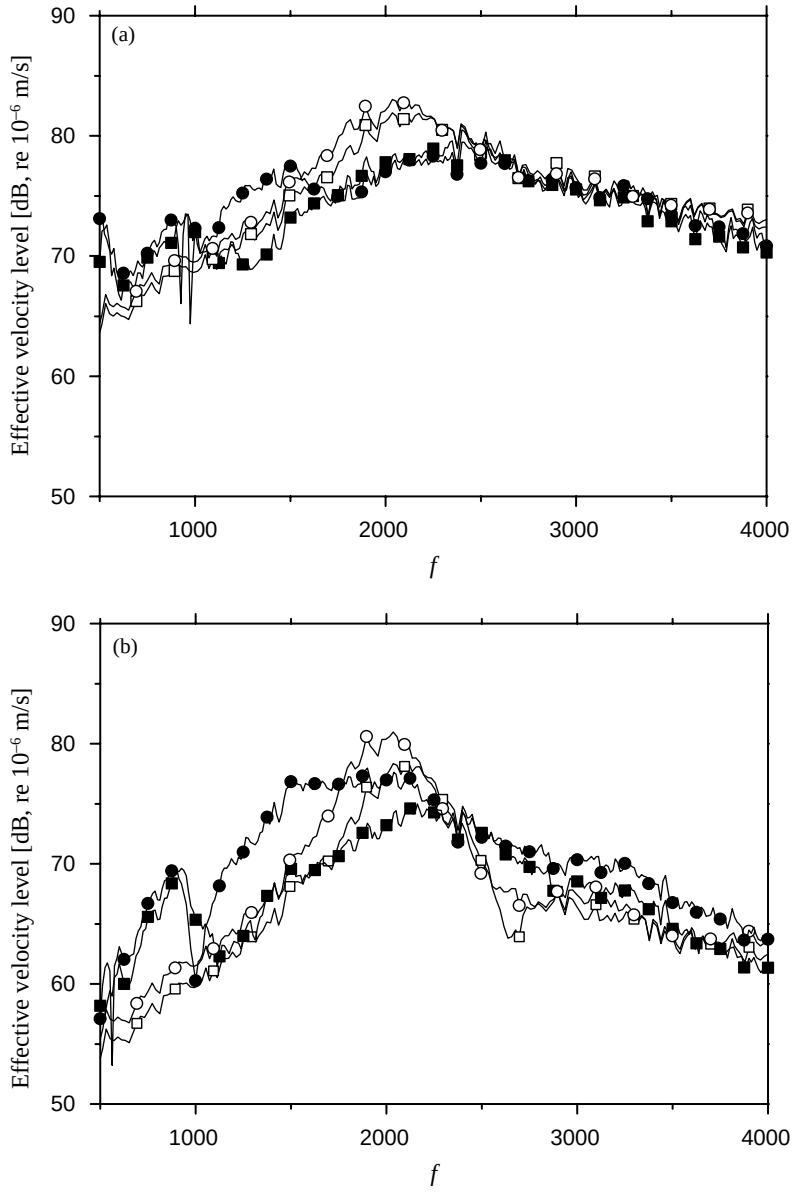

Figure 15. Effective transverse velocity level of the bulb seal on (a) the source side and (b) the receiver side. —■—, measured; —□—, calculated for $CR = 22{\cdot}5\%$; —●—, measured; —○—, calculated for $CR = 16{\cdot}9\%$.

affected the response of the bulb seal in the mass-controlled region. This effect is due to attenuation of bending waves in the seal membranes at high frequencies. The loss factor had negligible effects in the stiffness-controlled region.

5. DISCUSSION

In general, satisfactory agreement was obtained between the experimental data and the FE-analysis predictions (Figure 16). Systematic discrepancies were observed however,

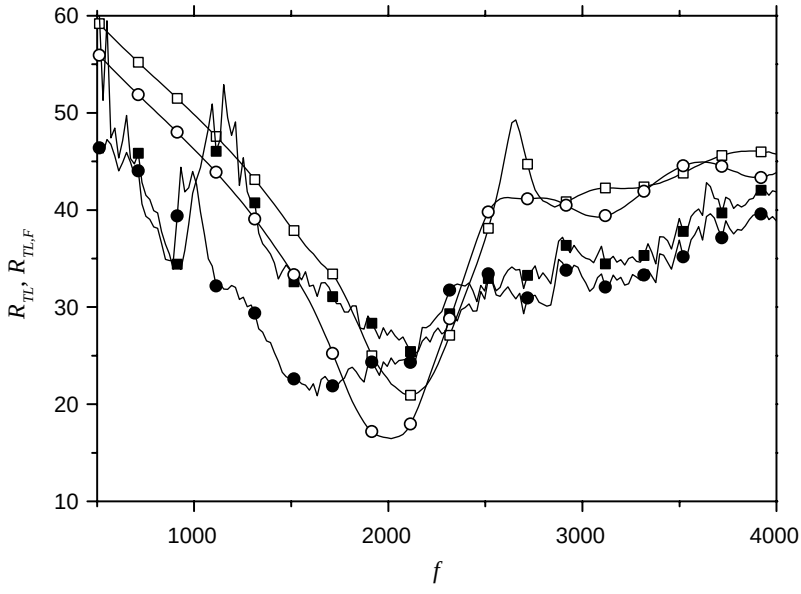

Figure 16. Sound transmission loss of the bulb seal determined from surface intensity measurements and comparison with numerical results. —■—, measured; —□—, calculated for $CR = 22{\cdot}5\%$; —●—, measured; —○—, calculated for $CR = 16{\cdot}9\%$.

which could not be fully explained. The predicted sound transmission loss values were lower than the measured values around resonance. This trend was reversed in other frequency regions. This could be in part due to the limitations of two-dimensional models. Possible three-dimensional behaviors in the experiments included: (1) reverberant sound fields, (2) the vibration of the seal in the y direction, (3) anisotropic material properties, and (4) the finite length of the seal sample and end corrections. To resolve these problems, a three-dimensional model of the bulb seal is necessary, which might require additional computational and modelling efforts.

The variability between seal samples was not taken into account, which is a serious shortcoming of the experiments. Recent studies in the automotive industry have demonstrated the importance of taking variability in dynamic frequency responses between nominally identical components into consideration before attempting comparisons with numerical predictions. This was not done here because of time and cost considerations. However, attempts will be made to address this important question in the future.

The assumption of fixed boundaries at the contacting nodes between the bulb and the mating block may be debatable. In reality, frictional forces at the contacting surface vary depending on the residual stress distribution in the seal and the deflected seal shape. Slippage between the seal and the mating block can occur in actual installations, depending on the magnitude of the friction coefficient.

6. CONCLUSIONS

The sound transmission characteristic and the vibration response of automotive foamed rubber bulb seals were investigated numerically and experimentally. The effects of material

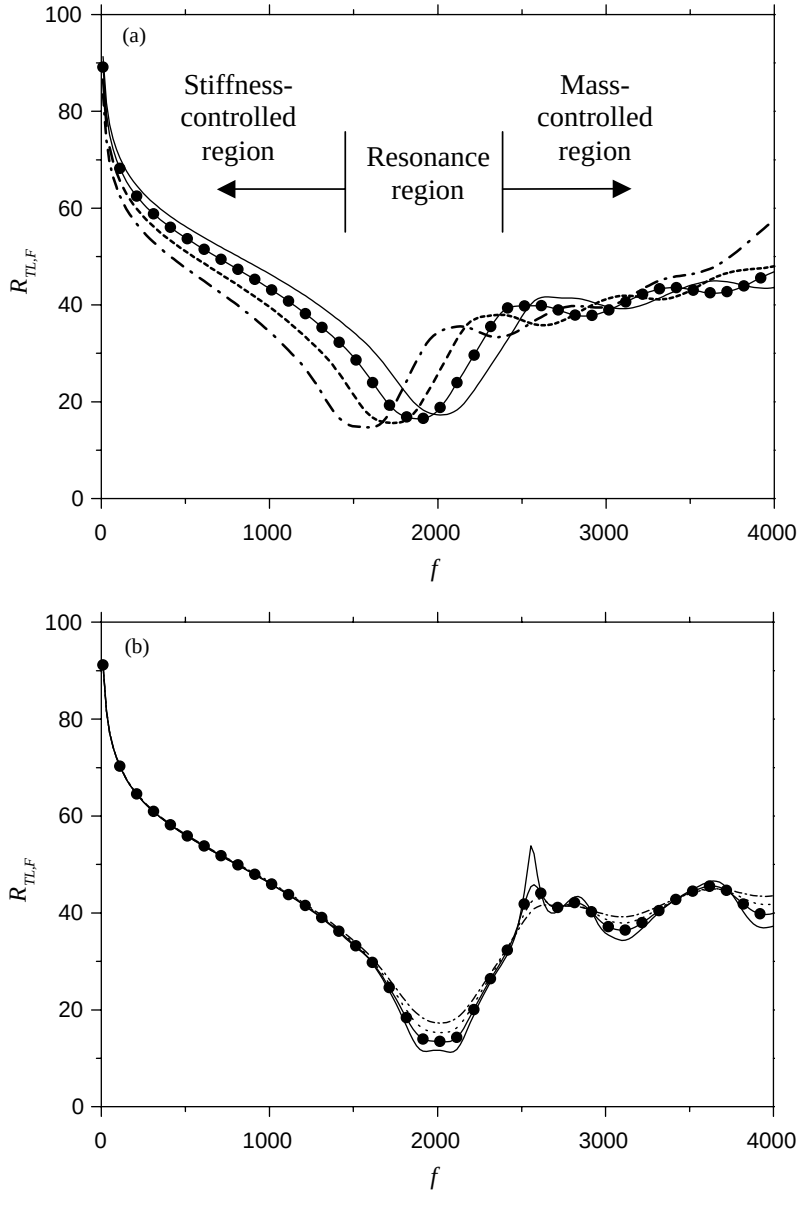

Figure 17. Effects of the seal material properties on the sound transmission loss of the bulb seal. (a) Effects of the nominal stiffness: ———, 2·3 MPa; —●—, 2·0 MPa; – – – –, 1·6 MPa; –·–·–, 1·3 MPa; (b) Effects of the loss factor, η: ———, 0·07; —●—, 0·10; – – – –, 0·13; –·–·–, 0·164.

properties and seal compression ratio were investigated. The main feature of the sound transmission characteristic of the bulb seals was found to be the existence of a mass–air–mass resonance frequency which depends on the compression ratio. For the seal sample used in the experiments, the mass–air–mass resonance frequency was around 2000 Hz. Surface acoustic intensity measurements indicated that more than 90% of the net energy absorbed by the seal was dissipated through mechanical damping. The rest of the absorbed energy was dissipated by sound wave radiation.

The sound transmission characteristics of the bulb seals were predicted using numerical models and compared with experimental data. It was found that the FE-model allowed the main trends in the sound transmission loss to be predicted for moderate seal compression ratios. The analysis clearly demonstrated that the frequency-dependent sound transmission loss of the bulb seal could be divided into three distinct regions: stiffness-controlled region, mass–air–mass resonance region, and mass-controlled region. Different seal design parameters such as the seal material properties, seal geometry, and contact area had a limited influence on the response in each of these regions. The loss factor directly influenced the sound transmission loss in the mass–air–mass resonance region. The contact area and the elastic properties of the seal material had major influences on the stiffness-controlled region and the value of the resonance frequency. The mass–air–mass resonance frequency could be predicted using a lumped element model. This suggested that a static FE-analysis could be used as a tool for representing a bulb seal system using a lumped element model and extracting model constants, which are strongly dependent on the seal shape and material properties. While in this paper the analysis was restricted to one primary bulb seal, the analysis procedures could be applied to other types of vehicle seals with minor adjustments.

ACKNOWLEDGMENTS

The authors express their thanks to Ford Motor Company and Advanced Elastomer Systems for their financial support and their guidance throughout this project. The contribution of the Herrick Laboratories Technical staff is also gratefully acknowledged.

REFERENCES

1. A. R. George and J. R. Callister 1991 *SAE General Aviation Meeting*, *Wichita, KS, Paper No*. 911027, 1–28. Aerodynamic noise of ground vehicles.
2. F. Fahy 1985 *Sound and Structural Vibration: Radiation, Transmission and Response*. London: Academic Press.
3. M. C. Gomperts 1964 *Acustica* **14**, 1–16. The "sound insulation" of circular and slit-shaped apertures.
4. G. P. Wilson and W. W. Soroka 1965 *Journal of the Acoustical Society of America* **37**, 286–297. Approximation to the diffraction of sound by a circular aperture in a rigid wall of finite thickness.
5. F. P. Mechel 1986 *Journal of Sound and Vibration* **111**, 297–336. The acoustic sealing of holes and slits in walls.
6. D. J. Oldham and X. Zhao 1993 *Journal of Sound and Vibration* **161**, 119–135. Measurement of the sound transmission loss of circular and slit-shaped apertures in rigid walls of finite thickness by intensimetry.
7. V. Hongisto 2000 *Journal of Sound and Vibration* **230**, 133–148. Sound insulation of doors—Part 1: prediction models for structural and leak transmission.
8. V. Hongisto, J. Keränen and M. Lindgren 2000 *Journal of Sound and Vibration* **230**, 149–170. Sound insulation of doors—Part 2: comparison between measurement results and predictions.
9. Y. Gur and K. N. Morman 1999 *Proceedings of the* 1999 *SAE Noise & Vibration Conference*, *Traverse City, MI*, *Paper No*. 1999-01-1804, 1187–1196. Sound transmission analysis of vehicle door sealing system.
10. G. S. Strumolo 1997 *Proceedings of the* 1997 *SAE Noise & Vibration Conference*, *Traverse City, MI*, *Paper No.* 971921, 417–425. The wind noise modeler.
11. R. Buchheim, W. Dobrzynski, H. Mankau and D. Schwabe 1982 *International Journal of Vehicle Design* **3**, 398–410. Vehicle interior noise related to external aerodynamics.

12. J. Y. Her, M. Lian, J. J. Lee and J. Moore 1997 *Proceedings of the* 1997 *SAE Noise & Vibration Conference*, *Traverse City, MI*, *Paper No.* 971922, 427–438. Experimental assessment of wind noise contributors to interior noise.
13. L. Mongeau and R. Danforth 1997 *SAE Transactions, Journal of Passenger Cars* **106**, 2668–2674. Sound transmission through primary bulb rubber sealing systems.
14. L. Mongeau, R. Danforth, S. C. Wood and C. J. Kessen 1996 *SAE Paper No.* 960193, in *Advances in Component Designs for Noise and Vibration Control*, SP-1147, 51–60. Laboratory method for evaluating the sound transmission characteristics of primary bulb body seals.
15. L. Mongeau, F. Han, Y. Champoux, D. Li and D. Iacovoni 1998 *Proceedings of the NOISE-CON' 98*, *Ypsilanti, MI*, 217–222. Robust design of vehicle weather sealing systems for minimal sound transmission.
16. J. Park, L. G. Mongeau and T. Siegmund 2000 *Proceedings of Acoustics Week in Canada* 2000, *Sherbrooke, Canada*, Vol. **28**, 102–103. Sound transmission characteristic of elastomeric sealing systems.
17. J. Park, L. G. Mongeau and T. Siegmund 2000 *Proceedings of the NOISE-CON 2000*, *Newport Beach, CA, Paper No:* 2*pNSc*3. Sound transmission loss of bulb seals.
18. F. J. Fahy 1995 *Sound Intensity*. London: E & FN Spon.
19. Polytec GmbH 1999 Vibrometer Operator's Manual for Polytec Vibrometer Series 3000. Waldbronn, Germany: Polytec GmbH.
20. D. A. Bies and C. H. Hansen 1996 *Engineering Noise Control*. London: E & FN Spon.
21. J. D. Ferry 1980 *Viscoelastic Properties of Polymers*. New York: John Wiley & Sons.
22. K. N. Morman Jr and J.C. Nagtegaal 1983 *International Journal for Numerical Methods in Engineering* **19**, 1079–1103. Finite element analysis of sinusoidal small-amplitude vibrations in deformed viscoelastic solids. Part I: theoretical development.
23. Hibbit Karlsson & Sorensen, Inc. 1998 *ABAQUS/Standard User's Manual*, Version 5.8. Pawtucket, Rhode Island: Hibbit Karlsson & Sorensen, Inc.
24. L. Cremer and M. Heckl 1988 *Structure-Borne Sound*. New York: Springer-Verlag.